Constitutive Androstane Receptor induces Ribonucleotide Reductase-M2 expression and maintains hepatocyte ploidy in mice

Anjana Asokakumar[1*], Bhoomika Mathur[1*], Anthony Chau[1], Bea Cronologia[1], Frances Alencastro[3], Linda Wheeler[2], Christopher K. Mathews[2], David D. Moore[4], Andrew W. Duncan[3], and Sayeepriyadarshini Anakk[1, 5, 6, §]

[1]Department of Molecular and Integrative Physiology, University of Illinois at Urbana-Champaign, Champaign, IL, USA, [2]Department of Biochemistry and Biophysics, Oregon State University, Oregon, USA, [3]Department of Pathology, Pittsburgh Liver Research Center, University of Pittsburgh, Pittsburgh, Pennsylvania, USA, [4]Nutritional Science and Toxicology, University of California, Berkeley, USA, , [5]Division of Nutritional Sciences, [6]Cancer Center at Illinois, University of Illinois at Urbana-Champaign, Champaign, IL,, USA.

* Co-first authors, [§]Corresponding author: anakk@illinois.edu

Abstract

The nuclear receptor Constitutive Androstane Receptor (CAR/NR1i3) is known for regulating various liver functions, including detoxification, nutrient metabolism, and hepatocyte proliferation. While CAR activation has been previously linked to higher ploidy, the underlying mechanisms are not fully known. Here, we uncover a basal role for CAR in maintaining hepatocyte ploidy, such that CAR deletion increases the number of diploid (2c) hepatocytes with a concomitant reduction in tetraploid (4c) hepatocytes. We demonstrate that CAR controls the *de novo* dNTP synthesis by directly transactivating the Ribonucleotide reductase-M2 (*RRM2*) gene, which encodes the rate-limiting catalytic subunit of the enzyme, ribonucleotide reductase. Further, we find that the ligand-dependent CAR activation is sufficient to induce several genes involved in the *de novo* dNTP synthesis pathways, resulting in higher hepatic dATP and dTTP levels within the liver. Importantly, overexpressing RRM2 levels in CAR knockouts led to increased DNA synthesis and tetraploid (4c) hepatocytes compared to the control mice. Taken together, these findings reveal that the CAR-mediated RRM2 regulation contributes towards DNA synthesis and thereby maintains hepatocyte ploidy.

Introduction

The liver is a metabolic hub and is responsible for many cellular functions[1,2]. Hepatocytes carry out detoxification and intermediary metabolism and comprise 70-80% of the liver tissue[3–5]. A salient feature of the hepatocytes is that they exhibit polyploidy[6]. Immature developing hepatocytes during the postnatal period (<21 days) are preferentially diploid, while the mature hepatocytes are more polyploid[6,7]. In rodents, polyploidization starts around the time of weaning, resulting in 80-90% of adult hepatocytes being polyploid[6]. Some studies have indicated a higher proliferation rate for diploid hepatocytes than polyploid hepatocytes[8,9]. Contrastingly, other studies demonstrate that higher hepatocyte polyploidy supports the adaptations during chronic liver injury or cancer by providing extra gene copies[6–8]. Nonetheless, polyploidy is conserved in the liver, but the mechanisms that link some of the metabolic functions, such as detoxification, to polyploidy remain elusive.

A key xenosensor in the liver that transcriptionally regulates detox machinery is the Constitutive Androstane Receptor (CAR or Nr1i3)[10]. Upon activation, CAR translocates to the nucleus, heterodimerizes with the Retinoid X receptor (RXR), and binds the xenobiotic response element module (XREM) of the target genes[11–13]. Besides detoxification, ligand-mediated CAR activation is typically accompanied by hepatomegaly and increased DNA synthesis as measured by Ki-67[14,15]. Moreover, synthetic CAR activators, TCPOBOP (TC), and phenobarbital have been shown to increase hepatocyte ploidy[14]. However, how these cells respond to these CAR-mediated increases in DNA synthesis and increases in dNTP requirements has not been fully examined.

We mined the publicly available transcriptome after CAR activation and found a robust increase in *RRM2* (Ribonucleotide Reductase Regulatory subunit M2) transcripts. This gene encodes the catalytic subunit of the rate-limiting enzyme ribonucleotide reductase, which converts NDPs (Nucleoside diphosphates) to dNDPs (deoxynucleoside diphosphates) in the dNTP synthesis pathway[16,17]. Then, we investigated if CAR could bind and activate RRM2 transcription and scanned the 5' upstream region of the RRM2 gene. We performed luciferase and chromatin immunoprecipitation assays, followed by PCR to validate the functionality of the putative CAR binding site. We measured hepatic dNTP levels to corroborate our findings.

59 Finally, ectopic expression of RRM2 in CAR knockouts (CARKO) was sufficient to alter DNA
60 synthesis and ploidy status in the hepatocytes.

61 **Results**

62 **Loss of CAR alters 2c and 4c ploidy status in the hepatocytes.**

63 As expected, CAR activation by TC results in an increased Ki-67 staining, hepatomegaly,
64 and robust induction of its downstream target genes, including *Cyp2b10,* Cyclin A (*CcnA*), and
65 Cyclin B (*CcnB*) in the liver[18,19], and these responses are absent in the global CAR knockout
66 mice (CARKO) (Fig 1A, SI Fig 1 A-G). Besides these known targets, we found that the E2F
67 family of transcription factors (*E2f1* and *E2f8*), responsible for controlling liver polyploidization,
68 are upregulated in a CAR-dependent manner (Fig 1 B-C). Similarly, the transcript levels of
69 Aurora Kinase B (*AurkB*) and Polo-like kinase1 (*Plk1*), genes responsible for the mitotic entry,
70 are increased upon CAR activation[20] (SI Fig 1 H-I). These findings highlight a key role for CAR
71 in regulating hepatic polyploidy. Next, we examined the cellular ploidy of 5-week-old male WT
72 and CARKO hepatocytes and found that deletion of CAR resulted in higher 2c content that
73 correlated with the reduction in 4c content. However, 8c and 16c proportions, which account for
74 ~20-30% of the polyploid state, were not altered (Fig 1D-F). Taken together, these findings
75 suggest that CAR regulates transcriptional regulators of ploidy and is necessary to maintain 2c
76 and 4c-hepatocyte ratios (~70-80% of ploidy states) and their distribution.

77

78 **CAR regulates the transcription of *Rrm2* gene.**

79

80 To investigate the mechanisms by which CAR activation promotes DNA synthesis and
81 subsequently ploidy, we mined the publicly available CAR transcriptome accessible through the
82 Nuclear Receptor Signaling Website Atlas (NURSA)
83 (http://signalingpathways.org/datasets/dataset.jsf?doi=10.1621/datasets.01003). Unexpectedly,
84 we noted an induction in ribonucleotide reductase subunits- *Rrm1* and *Rrm2* in response to TC
85 treatment. The *Rrm1* gene encodes the substrate-binding domain, while the *Rrm2* gene encodes
86 the catalytic subunit of the rate-limiting enzyme in the *de novo* dNTP synthesis pathway -

87 Ribonucleotide reductase[17]. We validated CAR-mediated induction of *Rrm1* and *Rrm2* transcripts
88 (Fig 2 A-B). Whereas the alternative subunit, *Rrm2b,* induced in response to DNA damage[17,21]
89 was downregulated (Fig 2C). We also found that only the RRM2 protein was increased upon
90 CAR activation, not RRM1 (Fig 2D). These upregulations were absent in the TC-treated
91 CARKO mice, suggesting CAR was necessary for these transcript and protein changes.

92 Based on these findings, we examined whether CAR directly regulates *Rrm2*
93 transcription. We screened the *Rrm2* promoter regions and identified putative CAR binding sites.
94 The putative CAR-binding DR3 motif (AGGT/GCA)[19] that was present 600 bp upstream in the
95 *Rrm2* promoter region was then cloned into the pTK-Luc vector (Fig 2E) to test its functionality
96 using luciferase assay. CAR activation with TC led to a significant increase in luciferase activity,
97 which was lost when this DR3 site on *Rrm2* was mutated (Fig 2F), confirming the transcriptional
98 activation. We then tested if CAR directly binds to the *Rrm2* promoter region using a chromatin
99 immunoprecipitation PCR (ChIP-PCR). FLAG-tagged-CAR transfected HepG2 cells were
100 treated with TC, and CAR was pulled down using the FLAG antibody. ChIP-PCR analysis
101 showed that ectopic expression of CAR was sufficient to allow its binding to the *Rrm2* gene (Fig
102 2 G-H) irrespective of the presence or absence of TC. These results demonstrate that the CAR
103 can bind and promote the transcription of the *Rrm2* gene.

104

105 **Activation of CAR upregulates the *de novo* dNTP synthesis pathway.**

106

107 We then tested if CAR activation regulated other genes encoding enzymes in the *de novo*
108 dNTP synthesis pathway besides the rate-limiting catalytic subunit of ribonucleotide reductase,
109 *Rrm2*. This pathway includes several steps, with ATIC (5-aminoimidazole-4-carboxamide
110 ribonucleotide formyltransferase/IMP cyclohydrolase) and UMP synthase (Uridine
111 monophosphate) being responsible for *de novo* purine and pyrimidine biosynthesis pathways,
112 respectively[22,23]. Briefly, IMPs are converted to ADPs (Adenose diphosphate) or GDPs
113 (Guanosine diphosphate), while UMPs are converted to UDP (Uridine diphosphate) and to UTP
114 (Uridine triphosphate), which is then acted upon by CTP synthetase to generate CTP (Cytidine
115 triphosphate). Ribonucleotide reductase subsequently reduces these substrates to their respective
116 dNDPs (deoxynucleoside diphosphate)[24]. dCMP deaminase enzyme keeps the pyrimidine dNTP

117 pool by converting dCMP to dUMP[25], which in turn can be further modified to dTDP by
118 deoxythymidylate (dTMP) kinase and finally to dNTPs via NDP (nucleoside diphosphate) kinase
119 (Figure 3 A).

120 TC treatment in WT mice resulted in the upregulation of transcripts encoding for these
121 key enzymes – AITC, UMP synthase, CTP synthetase, NDP kinase, dCMP deaminase, and
122 dTMP kinase in the liver (Figure 3 B-G). Despite the CAR-independent increase in NDP kinase,
123 induction of other enzymes was lost in the CARKO, indicating CAR dependency and
124 highlighting that CAR may regulate the expression of genes in the entire dNTP synthesis
125 pathway. Based on these results, we examined the dNTP pools in the liver tissue with and
126 without CAR activation. Consistent with the transcriptional data, dATP and dTTP levels were
127 robustly induced in a CAR-dependent manner (Figure 3 H and J). Unsurprisingly, the dCTP and
128 dGTP levels were unchanged since higher GTP levels are associated with increased liver
129 mitochondria[25,26] (Figure 3I). Whereas dCTP levels may be converted to dTTP due to increase
130 dCMP deaminase transcript (Figure 3 K). Collectively, these results uncover that CAR activation
131 upregulates dNTP synthesis genes and certain dNTP pools.

132

133 **Ectopic RRM2 expression induces DNA synthesis and alters ploidy in CARKO hepatocytes.**

134

135 Since RRM2 mediates the rate-limiting step for *de novo* dNTP synthesis[27], we examined
136 whether overexpressing (OE) RRM2 in the CARKO mice can compensate for ploidy loss and
137 promote DNA synthesis. Using AAV machinery, we introduced a 10^11 GC virus carrying
138 RRM2-GFP or Control-GFP construct into the mice and ensured that this did not cause overt
139 inflammation (SI Fig 2 A-D). As expected, compared to the control-GFP virus, RRM2-AAV led
140 to a robust increase in *Rrm2* mRNA in WT and CARKO mice, ~10 fold and 6 fold respectively
141 (Fig 4 A). Importantly, RRM2 overexpression did not change the *Rrm2b* or *Rrm1* transcript
142 levels in both WT and CARKO mice, indicative of specificity of this overexpression with no
143 compensatory impact on other subunits (SI 2 E-F). We validated the RRM2-GFP expression in
144 the livers of WT and CARKO mice by imaging isolated primary hepatocytes. Despite a lower

145 fold increase in *Rrm2* transcript levels in CARKO, we observed no significant change in the
146 RRM2-GFP expression compared to WT. (Fig 4 C)

147 Nonetheless, we were surprised to notice an 18% increase in the liver-to-body weight
148 ratio in CARKOs but not in the WT mice (Fig 4 B, SI Fig 2 G-H). To examine if there was
149 excessive DNA synthesis upon RRM2 OE in CARKO, we used the DNA synthesis marker, Ki-
150 67[28]. RRM2 OE dramatically increased the percentage of Ki-67 positive nuclei, specifically in
151 CARKO (~2 fold) compared to WT mice (Fig 4 D-E, SI Fig 3A-D). Intriguingly, despite higher
152 Ki-67 staining, the total number of cells in the given microscopic field in CARKO was lower
153 (Fig 4 F). Furthermore, when we measured the hepatocyte cellular area on RRM2 OE using β-
154 catenin staining, CARKO exhibited larger hepatocytes compared to WT (Fig 4 G, SI Fig 3 E-H).
155 Overall, these experiments show that introducing RRM2 in CARKO is sufficient to increase
156 DNA synthesis, cellular area, and, subsequently, the hepatosomatic index (liver-to-body weight
157 ratio).

158 In WT adult mouse livers, approximately 80-90% of hepatocytes are polyploid. Further,
159 hepatocytes can be mono- or binucleate, resulting in varying cellular and nuclear ploidy[7,29]. For
160 instance, a tetraploid can be 4c in a mononucleate or 2c in a binucleate cell; an octoploid can be
161 8c in a mononucleate or 4c in a binucleate cell, and so on. Hence, the percentage of 2c in nuclear
162 ploidy analysis will be higher than the cellular ploidy. As expected, nuclear ploidy distribution
163 differs from the cellular ploidy shown earlier. In nuclear ploidy, 2c and 4c nuclear content
164 comprises ≥90 percent of all the nuclei. Nuclear ploidy was assessed in frozen liver samples that
165 were also used for transcriptional analysis elsewhere. RRM2 OE in WT mice did not alter
166 nuclear ploidy status in the hepatocytes (SI Fig 4 A, C). However, in the CARKO hepatocytes,
167 RRM2 OE restored the nuclear 2c and 4c to WT levels (SI Fig 4 B-C). This data is consistent, as
168 most tetraploid hepatocytes (70-80%) are binucleate with diploid nuclei, which explains the
169 increase in 2c nuclei in the CARKO RRM2 OE group. Likewise, as most octoploid hepatocytes
170 are binucleate with tetraploid nuclei, this may lead to a decrease in 4c nuclei.

171 Additionally, in a separate cohort of mice, we also determined cellular ploidy after RRM2
172 OE. Unlike 5-week-old mice, whose livers are still maturing, 16-week-old adult livers are in a
173 quiescent state and exhibit a different ploidy distribution. Although the percentage of 2c and 4c
174 hepatocytes in 5-week-old and 16-week-old WT were comparable, the adult mice displayed more

175 8c and 16c hepatocytes (Fig 1 E, G and Fig 4 H, J). This is consistent with older mice displaying
176 increased 8c with a concomitant decrease in 4c hepatocytes (SI Fig 4D). In the CARKOs, we
177 noticed that 2c hepatocytes significantly dropped with aging from 14.1% to 4.3% (Fig 1 F, G and
178 Fig 4 I, J), indicating that ploidy "catches up" over time.

179 Although RRM2 OE increased the number of 2c hepatocytes in both genotypes, this
180 increase was insignificant. However, ectopic expression of RRM2 in CARKO increased the
181 percentage of 4c and 8c hepatocytes. Both these changes in the CARKO were comparable to
182 those of WT mice treated with RRM2. Nonetheless, RRM2 OE in CARKO results in higher Ki-
183 67 staining, increased 2c nuclei, and increased 2c hepatocytes.

184 Since ploidy can be altered with pathological conditions[7,29], we examined whether this
185 change in the ploidy seen in WT and CARKO post-RRM2 OE was pathological by tunnel and
186 H2Ax staining for DNA damage. We found no immunostaining differences between the control
187 and RRM2 OE, negating the role of pathological ploidy changes; rather, they are driven by
188 RRM2 OE (SI Fig 4 E, F). Collectively, these data suggest that the CAR contributes towards
189 dNTP synthesis and hepatocyte ploidy via RRM2.

190

191 **Discussion**

192

193 In rodents, transient CAR activation results in hepatomegaly, increased Ki-67 staining,
194 and is linked to higher polyploidy, while prolonged activation results in liver cancer[14,30].
195 Although *FoxM1, Mdm2,* and *cMyc* signaling are implicated in facilitating CAR-driven liver
196 proliferation, how CAR orchestrates DNA synthesis and ploidy remains unknown. Here, we
197 identified a new CAR target, *Rrm2*, which encodes the catalytic subunit of the ribonucleotide
198 reductase complex that is essential for *de novo* dNTP synthesis. Additionally, ligand activation of
199 CAR was sufficient to induce several genes involved in dNTP biosynthesis. All these effects
200 were absent in CARKO mice. We have not investigated if all these dNTP biosynthesis genes are
201 direct or indirect targets of CAR. But one of the key rate-limiting steps is catalyzed by
202 ribonucleotide reductase, and we demonstrate that CAR directly regulates the RRM2 subunit.

203 With respect to ploidy, CAR has been thought to increase ploidy by facilitating the
204 endoreduplication of DNA[14]. Here, we show that CAR can regulate various aspects of hepatic
205 polyploidization. Intriguingly, we found that CAR activation induces the *E2f* family of
206 transcription factors that activate and inhibit polyploidization. For instance, *E2f1* promotes
207 polyploidization while *E2f*8 inhibits it. CAR may contribute to maintaining overall ploidy
208 distribution by inducing both pro- and anti-polyploidization regulators. Moreover, we find that
209 cytokinesis mediators- *Aurkb* and *Plk1* transcripts are also induced in a CAR-dependent manner.
210 These results underscore an overarching role for CAR in controlling several aspects of liver
211 polyploidization, from DNA synthesis to E2F transcriptional network to cytokinesis regulators.

212 We validated that dNTP levels in livers were higher post-CAR activation, which is
213 consistent with the *Rrm2* gene and protein induction. We find a significant increase in dATP and
214 dTTP levels. dATP, in turn, can act as an allosteric inhibitor of RRM2 activity[31]. Thus, RRM2
215 expression and activity are tightly controlled. One possibility is that the RRM2 increase seen in
216 TC treatment is secondary to cell cycle activation to promote DNA synthesis. So, we tested the
217 consequence of OE of RRM2 in quiescent CARKO livers from adult mice. We note that control
218 viral injections, as expected, result in a mild pro-proliferative response in both genotypes. While
219 RRM2 OE in WT led to staining of Ki-67 comparable to that of GFP virus-treated mice, in
220 CARKO, it robustly amplified the Ki-67 staining, indicating increased DNA synthesis in
221 CARKO. This data implies that in the absence of CAR, RRM2 OE is sufficient to increase DNA
222 synthesis and alter ploidy and overall liver size. Since there are compensatory effects by other
223 RRM subunits, especially *Rrm2b*, we measured *Rrm1* and *Rrm2b* and found their levels
224 unchanged upon RRM2 OE (SI Fig 2 E-F).

225 A limitation of this study is that we do not fully understand how RRM2 OE promotes this
226 heightened DNA synthesis response in CARKOs. First, we examined the transcripts involved in
227 the dNTP synthesis pathway. Post RRM2 OE, there was no change except for a reduction in
228 UMP synthetase and dTMP kinase transcripts, indicative of a potential compensatory effect (SI
229 Fig 5 A—F). Similarly, cell cycle pathway genes were examined, and we found that S phase
230 cyclins—*Ccna1* and *Ccne1*, were increased in CARKO (SI Fig 5 G-H), which is consistent with
231 higher Ki-67 staining. However, the *E2f1* and *E2f8* transcripts did not change post-RRM2 OE in
232 WT and CARKO livers (SI Fig 5 I-J). These findings indicate that the ectopic introduction of

233 RRM2 is sufficient to alter genes involved in the *de novo* dNTP biosynthesis pathway and S-
234 phase cyclins, mainly in CARKO.

235 In terms of ploidy, RRM2 OE in the absence of CAR increased diploid nuclear content
236 that coincided with the decrease in tetraploid nuclear content (SI Fig 4B-C). The cellular ploidy
237 of CARKO RRM2 OE mimicked that of WT RRM2 OE, suggesting the CAR-mediated RRM2
238 expression is essential in maintaining the liver ploidy status (Fig 4 H -I, SI Fig 4 A-C).
239 Moreover, our cellular ploidy at different time points in CARKO (5 weeks vs. 16 weeks) implies
240 that the loss of CAR may delay polyploidization, which may normalize with aging (Fig 1E-G,
241 Fig 4 H-J).

242 Polyploid hepatocytes have been shown to have a distinct metabolic capacity[7,8,32] and are
243 in line with xenosensing function of CAR. Putting all the findings together, we demonstrate that
244 CAR-RRM2 signaling may coordinate liver proliferation and polyploidy status and that CAR
245 may play a basal role in maintaining liver ploidy status during development.

246

247 **Method**

248

249 **Mice experiment** – C57BL/6J mice were obtained from Jackson laboratories and CARKO mice
250 were obtained from Dr Moore's lab at Baylor College of Medicine. The age and sex of the mice
251 used for the experiments are mentioned in the figure legends. The mice were housed in a
252 standard 12 -hr light/dark cycle with chow food and water ad libitum. All the mice used in the
253 study have complied with NIH guidelines for the care and use of laboratory animals and
254 experiments were performed as directed by the Institutional Animal Care and Use Committee at
255 the University of Illinois, Urbana-Champaign (UIUC, IACUC protocol: 22183). All mice were
256 acclimatized to the facility at least 2 weeks prior to the experiments. Mouse CAR agonist, 1,4-
257 bis[2-(3,5-dichloropyridyloxy)]benzene (TCPOBOP), TC was dissolved in Cornoil and
258 intraperitoneally (IP) injected at 100 mg/Kg once into the mice, euthanized after 3 days of
259 treatment, and collected samples for further studies. AAVDJ8 (VB220927-1597gxb and
260 VB220823-1142mex) viruses were obtained from the vector builder and were injected at a

261 concentration of 10^11 GC. The mice were euthanized after two weeks for serum and liver
262 collection.

263 **RNA extraction, cDNA synthesis, and qPCR** – RNA from the liver was isolated with TRIzol
264 (Invitrogen) using the manufacturer's instructions. The quality of the RNA was measured using
265 the Bioanalyzer and 0.2% bleach gel. 3-5 µg of isolated RNA was used to synthesize the cDNA
266 with random primers (NEBiolabs) and the Maxima Reverse transcriptase kit (Thermo Fisher
267 Scientific). 50 ng of cDNA was used for every SYBR green kit (Thermo Fisher Scientific) based
268 qRT-PCR. Relative gene expression was calculated by ΔCt or ΔΔCt method and normalized to
269 36b4 or actin as mentioned in the figure legends. qPCR primer details are listed in the
270 supplementary table.

271 **Western blot assay** – Protein lysates were made with RIPA buffer (25 mM Tris-HCl, 150 mM
272 NaCl, 0.5% Sodium deoxycholate, 1% Triton X-100, 0.1% SDS, 0.1 mL Phosphatase inhibitor,
273 and 1x protein inhibitor). A total of 50µg of liver tissue lysate was loaded to each lane and was
274 separated with 10% SDS-PAGE. The proteins were then transferred to a nitrocellulose
275 membrane. After blocking with 5% non-fat milk in TBS, the membrane was probed with a
276 primary antibody (GAPDH (Cell Signaling, #2118, 1:5000), RRM1 (Santa Cruz, sc-377426,
277 1:100), RRM2, (Santa Cruz, sc-81850, 1:100)) followed by a secondary antibody (1:5000,
278 Jackson Immunoresearch). The membrane was developed with Enhanced Chemiluminescent
279 detection reagent and imaged with X-Ray films.

280 **Luciferase assay** - In Vitro, HepG2 cells were transfected using calcium phosphate cotransfected
281 with 0.5 µg/well of both the luciferase reporter (mRRM2- pTK LUC) and beta-gal as internal
282 control plasmid and indicated amounts of receptor expression vectors[33]. 35 bp of the CAR
283 response element identified in the RRM2 promoter region was sequenced and cloned into TK-
284 LUC for analysis. The mutant RRM2 CAR response element was generated by mutating the key
285 GG nucleotides to AA. After transfection, the cells were treated with mouse constitutive
286 androstane receptor (mCAR): 250 nm overnight. Luciferase expression was assayed and
287 normalized using β-gal expression. All luciferase values were averaged from triplicate samples.
288 All transfection data were repeated at least three times.

289 **Chromatin Immuno-Precipitation (ChIP)** - FLAG-CAR protein was transiently transfected
290 into HepG2 cells. After 24 hours of TC treatment, the FLAG-tagged CAR was pulled down

291 using an anti-FLAG antibody (Sigma, F1840), followed by sonication and PCR amplification of
292 the RRM2 promoter region. All transfection data and pull-down experiments were performed in
293 three separate wells.

294 **Liver histology and staining** – Mouse liver tissues were fixed in 10% formalin for 12-24 hours,
295 processed, and embedded in paraffin. 5 µm liver sections were made and deparaffinized in
296 xylene and hydrated in a series of graded alcohol and water. Standard hematoxylin and eosin
297 (H&E) methods were used to examine the morphology. For immunohistochemistry (IHC),
298 sections were incubated with 3% hydrogen peroxide for 15 minutes to block endogenous
299 peroxidase. In both IHC and immunofluorescence (IF), the sections are heated in Tris-EDTA (pH
300 9.0) for 30 minutes for antigen retrieval, followed by 1 hour of blocking in 5% BSA and 2%
301 NGS at 4^0C. The sections were incubated with primary antibody Ki-67 (550609, BD Bioscience,
302 1:100 dilution), β-catenin (BDB610154, BD Bioscience, 1:1000 dilution), or H2A.X (ab11175,
303 abcam, 1:500) at 4^0C overnight. After the TBST wash, samples were incubated with horseradish
304 peroxidase (HRP) anti-mouse (company, 1:200 dilution) or anti-mouse fluorophore for an hour at
305 RT. For IHC, the DAB staining (Vectorbiolab) kit was used according to the manufacturer's
306 protocol. For IF, the sections were then incubated with NuBlue (ThermoScientific) for 30
307 minutes at room temperature, and the background signals were quenched using the Vector
308 TrueVIEW Autofluorescence Quenching (SP-8400-15) from the Vector Laboratories as per the
309 instructions. The slides were viewed with Nanozoomer or LSM 900.

310 **Hepatocyte isolation** – Hepatocytes were isolated as described in Wilkinson et al[8].

311 **Tunnel staining** – For checking the DNA damage, tunnel staining was performed with Click-iT™
312 Plus TUNEL Assay Kits (ThermoFisher Scientific, # C10617) as per the instructor's manual and
313 view them under LSM 900 microscope.

314 **Ploidy analysis** – For detection of cellular ploidy, freshly isolated primary hepatocytes were
315 stained with 2 µl/ml Fixable Viability Dye (FVD) eFluor 780 (eBioscience, San Diego, CA) and
316 15 µg/ml Hoechst 33342 (Life Technologies, Carlsbad, CA), as described[8]. For nuclear ploidy,
317 nuclei from the frozen liver tissue were isolated as previously described[9,34]. - A piece of frozen
318 liver tissue, approximately 5 x 5 x 3 mm, was thawed at room temperature in 1 mL of PBS and
319 chopped into tiny pieces with a scalpel blade. The liver suspension was passed through a 20-gauge
320 needle (10 times) and a 23-gauge needle (10 times) to break open cells. Suspensions were fixed

overnight in 70% ethanol at 4°C, washed with PBS, centrifuged at 500g for 5 minutes at 4°C, and digested in 1.5mL pepsin (0.5mg/mL in 0.1N HCl, Millipore Sigma Life Science) for 20 minutes at RT to generate nuclear suspensions. The nuclear suspensions were washed with 3 mL nuclear wash buffer (PBS, 0.1% BSA, 0.5% Tween-20), incubated with 1.5 mL 2N HCl for 12 minutes at 37°C, washed with 3mL cold borate buffer (6.25g H3BO3/L type I water, pH 8.5), and centrifuged at 500 g for 5 minutes at 4°C. The isolated nuclei were then stained with 5 µg/mL propidium iodide (Invitrogen, Carlsbad, CA) in PBS with 250 µg/mL RNase A (Invitrogen) and analyzed with an LSR II flow cytometer (BD Biosciences, Franklin Lakes, NJ) running BD FACSDiva™ Software pH v9.0. FACS plots were generated using FlowJo 10.8.2 (FlowJo LLC, Ashland, OR)

Qupath, image J software – Qupath is used to quantify the Ki-67 staining and count the number of cells. Image J software for cellular area analysis

Statistical analyses. All statistical analyses were performed using GraphPad PRISM (GraphPad Software, Inc., La Jolla, CA). Data are presented as mean ± standard deviation (SD) or mean ± standard error of the mean (SEM). Student unpaired T-test and Two-way ANOVA were performed, followed as described in the legends of figures. Level of significance was $*P < 0.05$, $**P < 0.01$, $***P < 0.001$.

Acknowledgements

This work was supported by NIH grants R01DK113080 (to SA) and R01DK103645 (to AWD). The University of Pittsburgh Unified Flow Core (RRID:SCR_025102), the Pittsburgh Liver Research Center Clinical Biospecimen and Processing Core (P30DK120531), Core Facilities at the Carl R. Woese Institute for Genomic Biology, and the Roy J. Carver Biotechnology Center at the UIUC supported this project. We would like to thank Dr Chang Cui, Department of Biochemistry, UIUC, for helping in critically interpreting RRM2 overexpression data. Emeritus Professor Christopher K Mathews helped us with the tissue dNTP levels.

Authors Contribution

A.A., B.M., and S.A. planned and designed the experiments for this study. D.M.D assists in transcriptional study design. B.M. and A.C. performed the *de novo* dNTP pathway analysis. L.W. and C.K.M. performed the dNTP analysis. F.A. and A.W.D. performed all the FACS sorting and ploidy data analysis. B.M., A.A. and B.C. isolated hepatocytes and nuclei for FACS analysis.

A.A. and S.A. designed and carried out the experiments for overexpression studies. A.A., A.W and S.A. wrote the manuscript with suggested edits by all the authors.

References

1. Forbes, S. J. & Newsome, P. N. Liver regeneration — mechanisms and models to clinical application. *Nat Rev Gastroenterol Hepatol* **13**, 473–485 (2016).
2. Michalopoulos, G. K. & Bhushan, B. Liver regeneration: biological and pathological mechanisms and implications. *Nature Reviews Gastroenterology & Hepatology* **18**, 40–55 (2021).
3. Bogdanos, D. P., Gao, B. & Gershwin, M. E. Liver Immunology. *Compr Physiol* **3**, 567–598 (2013).
4. Blouin, A., Bolender, R. P. & Weibel, E. R. Distribution of organelles and membranes between hepatocytes and nonhepatocytes in the rat liver parenchyma. A stereological study. *J Cell Biol* **72**, 441–455 (1977).
5. Mendoza, R. *et al.* Isolation and Culture of Mouse Hepatocytes and Kupffer Cells (KCs). *Methods Mol Biol* **2455**, 73–84 (2022).
6. Donne, R., Saroul-Aïnama, M., Cordier, P., Celton-Morizur, S. & Desdouets, C. Polyploidy in liver development, homeostasis and disease. *Nat Rev Gastroenterol Hepatol* **17**, 391–405 (2020).
7. Wang, M.-J., Chen, F., Lau, J. T. Y. & Hu, Y.-P. Hepatocyte polyploidization and its association with pathophysiological processes. *Cell Death Dis* **8**, e2805–e2805 (2017).
8. Wilkinson, P. D. *et al.* The Polyploid State Restricts Hepatocyte Proliferation and Liver Regeneration in Mice. *Hepatology* **69**, 1242–1258 (2019).

374 9. Pandit, S. K. *et al.* E2F8 is essential for polyploidization in mammalian cells. *Nat Cell Biol*
375 **14**, 1181–1191 (2012).
376 10. Wei, P., Zhang, J., Egan-Hafley, M., Liang, S. & Moore, D. D. The nuclear receptor CAR
377 mediates specific xenobiotic induction of drug metabolism. *Nature* **407**, 920–923 (2000).
378 11. Kawamoto, T. *et al.* Phenobarbital-Responsive Nuclear Translocation of the Receptor CAR
379 in Induction of the CYP2B Gene. *Molecular and Cellular Biology* **19**, 6318–6322 (1999).
380 12. Yoshinari, K., Kobayashi, K., Moore, R., Kawamoto, T. & Negishi, M. Identification of the
381 nuclear receptor CAR:HSP90 complex in mouse liver and recruitment of protein
382 phosphatase 2A in response to phenobarbital. *FEBS Letters* **548**, 17–20 (2003).
383 13. Kobayashi, K., Sueyoshi, T., Inoue, K., Moore, R. & Negishi, M. Cytoplasmic Accumulation
384 of the Nuclear Receptor CAR by a Tetratricopeptide Repeat Protein in HepG2 Cells. *Mol*
385 *Pharmacol* **64**, 1069–1075 (2003).
386 14. Huang, W. *et al.* Xenobiotic Stress Induces Hepatomegaly and Liver Tumors via the Nuclear
387 Receptor Constitutive Androstane Receptor. *Molecular Endocrinology* **19**, 1646–1653
388 (2005).
389 15. Shizu, R. *et al.* Xenobiotic-Induced Hepatocyte Proliferation Associated with Constitutive
390 Active/Androstane Receptor (CAR) or Peroxisome Proliferator-Activated Receptor α
391 (PPARα) Is Enhanced by Pregnane X Receptor (PXR) Activation in Mice. *PLOS ONE* **8**,
392 e61802 (2013).
393 16. Nordlund, P. & Reichard, P. Ribonucleotide Reductases. *Annual Review of Biochemistry* **75**,
394 681–706 (2006).
395 17. Aye, Y., Li, M., Long, M. J. C. & Weiss, R. S. Ribonucleotide reductase and cancer:
396 biological mechanisms and targeted therapies. *Oncogene* **34**, 2011–2021 (2015).

397 18. Yang, H. & Wang, H. Signaling control of the constitutive androstane receptor (CAR).
398 *Protein Cell* **5**, 113–123 (2014).
399 19. Mäkinen, J. *et al.* Modulation of Mouse and Human Phenobarbital-Responsive Enhancer
400 Module by Nuclear Receptors. *Mol Pharmacol* **62**, 366–378 (2002).
401 20. Goldenson, B. & Crispino, J. D. The Aurora Kinases in Cell Cycle and Leukemia. *Oncogene*
402 **34**, 537–545 (2015).
403 21. Tanaka, H. *et al.* A ribonucleotide reductase gene involved in a p53-dependent cell-cycle
404 checkpoint for DNA damage. *Nature* **404**, 42–49 (2000).
405 22. Buchanan, J. M. & Hartman, S. C. Enzymic Reactions in the Synthesis of the Purines. in
406 *Advances in Enzymology and Related Areas of Molecular Biology* 199–261 (John Wiley &
407 Sons, Ltd, 1959). doi:10.1002/9780470122662.ch5.
408 23. Rayl, E. A., Moroson, B. A. & Beardsley, G. P. The Human *pur*H Gene Product, 5-
409 Aminoimidazole-4-carboxamide Ribonucleotide Formyltransferase/IMP Cyclohydrolase.
410 *Journal of Biological Chemistry* **271**, 2225–2233 (1996).
411 24. Reichard, P. INTERACTIONS BETWEEN DEOXYRIBONUCLEOTIDE AND DNA
412 SYNTHESIS. *Annual Review of Biochemistry* **57**, 349–374 (1988).
413 25. Mathews, C. K. Deoxyribonucleotides as genetic and metabolic regulators. *The FASEB*
414 *Journal* **28**, 3832–3840 (2014).
415 26. Weibel, E. R., Stäubli, W., Gnägi, H. R. & Hess, F. A. Correlated morphometric and
416 biochemical studies on the liver cell. I. Morphometric model, stereologic methods, and
417 normal morphometric data for rat liver. *Journal of Cell Biology* **42**, 68–91 (1969).
418 27. Elledge, S. J., Zhou, Z. & Allen, J. B. Ribonucleotide reductase: regulation, regulation,
419 regulation. *Trends in Biochemical Sciences* **17**, 119–123 (1992).

420 28. Stamatiou, K. *et al.* Ki-67 is necessary during DNA replication for fork protection and
421 genome stability. *Genome Biology* **25**, 105 (2024).
422 29. Polyploidy in liver development, homeostasis and disease | Nature Reviews
423 Gastroenterology & Hepatology. https://www.nature.com/articles/s41575-020-0284-x.
424 30. Dong, B. *et al.* Activating CAR and β-catenin induces uncontrolled liver growth and
425 tumorigenesis. *Nature Communications* **6**, 5944 (2015).
426 31. Ando, N. *et al.* Allosteric Inhibition of Human Ribonucleotide Reductase by dATP Entails
427 the Stabilization of a Hexamer. *Biochemistry* **55**, 373–381 (2016).
428 32. Zhang, S. *et al.* The Polyploid State Plays a Tumor-Suppressive Role in the Liver.
429 *Developmental Cell* **47**, 390 (2018).
430 33. Lee, Y.-K., Parker, K. L., Choi, H.-S. & Moore, D. D. Activation of the Promoter of the
431 Orphan Receptor SHP by Orphan Receptors That Bind DNA as Monomers *. *Journal of*
432 *Biological Chemistry* **274**, 20869–20873 (1999).
433 34. Moreno, E. *et al.* Inhibition of polyploidization in Pten-deficient livers reduces steatosis.
434 *Liver Int* **42**, 2442–2452 (2022).
435
436

437 **Figures**

438

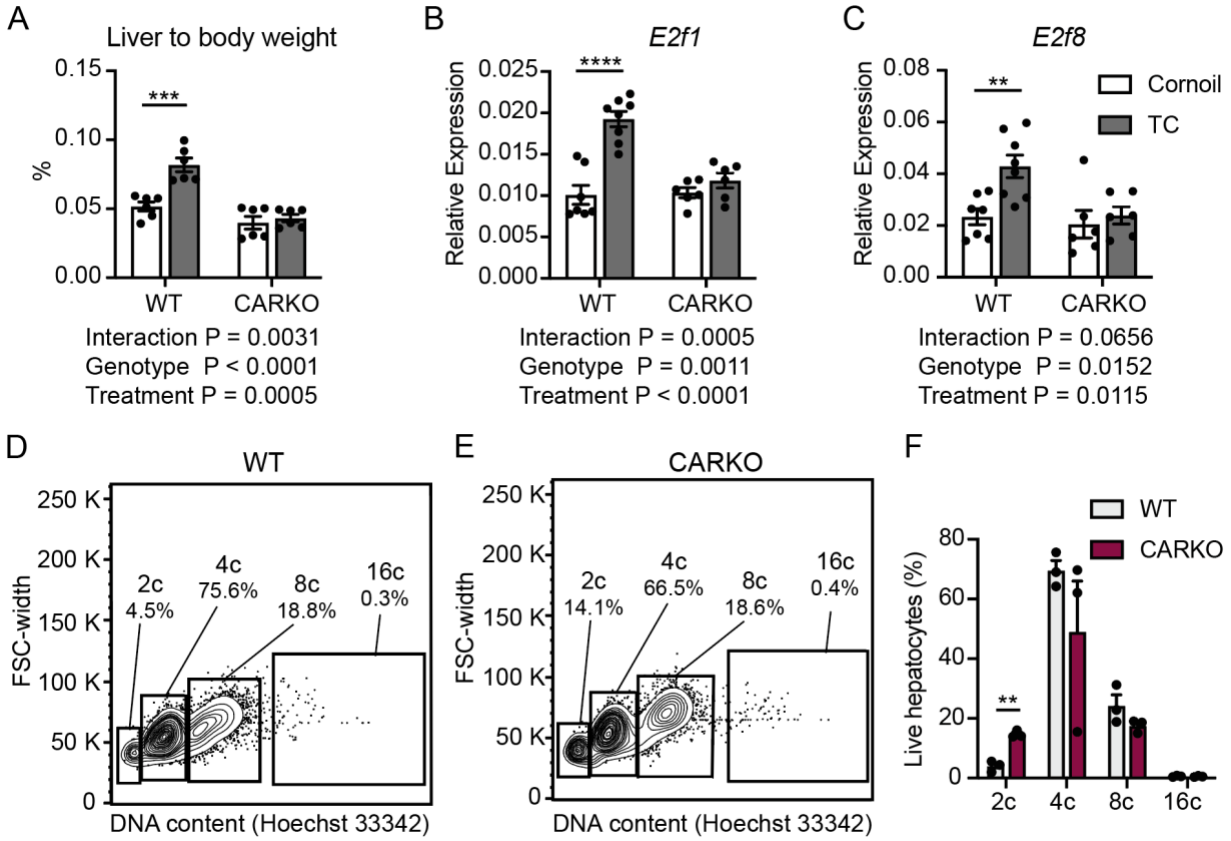

439

440 **Figure 1 - Loss of CAR disrupts the mouse hepatocyte ploidy.** (A) The liver-to-body weight
441 ratio of WT and CARKO mice on CAR activation with TC or with control (Cornoil). (B-C) The
442 transcript levels of ploidy-regulating genes *E12f1* and *E2f8* on CAR activation were analyzed
443 using qPCR (n = 6-8 mice/group, adult male mice, 3-month-old; 36b4 was used as the internal
444 control). 2-way ANOVA was performed for the statistical significance. (D and E) Isolated
445 hepatocytes were isolated from 5-week-old male mice, FACS sorted, and used for cellular ploidy
446 analysis. Representative images of gating channels for identifying the DNA content of WT (D)
447 and CARKO (E) hepatocytes. (G) Quantification of live hepatocytes obtained from cellular
448 ploidy analysis and unpaired two-tailed T-tests was used to perform the analysis, **p<0.005,
449 ***p<0.0005

450

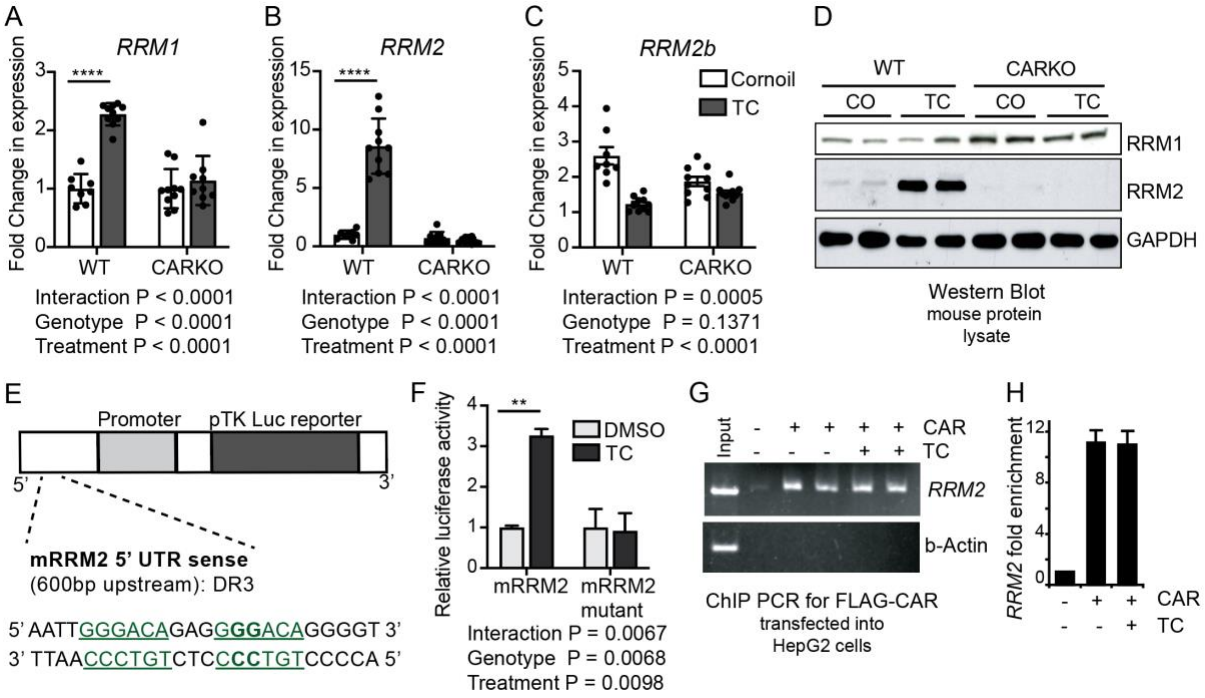

Figure 2 - CAR binds and transactivates *RRM2* expression. (A) Transcript expression levels of the ribonucleotide reductase subunit, *Rrm1* (A), and *Rrm2* (B) were analyzed using qPCR. (C) *Rrm2b*, an alternative subunit of ribonucleotide reductase transcript levels, was also measured using qPCR. (n = 8-10 mice/group, 3-month-old male mice, β-actin was used as the internal control for qPCR analysis). (D) Immunoblot analysis of the subunit proteins RRM1 and RRM2 in the mouse liver lysates with and without TC treatment. (E) Schematic representation of the luciferase assay and the target RRM2 site sequence used for the assay. The mutated sites for mRRM2 mutants are marked in **bold**. (F) Quantification for the luciferase assay of mRRM2 and mRRM2 mutant constructs transfected into the HepG2 cell line. (G-H) FLAG-tagged CAR construct was transfected to HepG2 cells, and the expressed FLAG-CAR proteins were pulled down to perform ChIP. ChIP-PCR was performed for the analysis (G) and quantified (H). (n = 3 technical replicate)

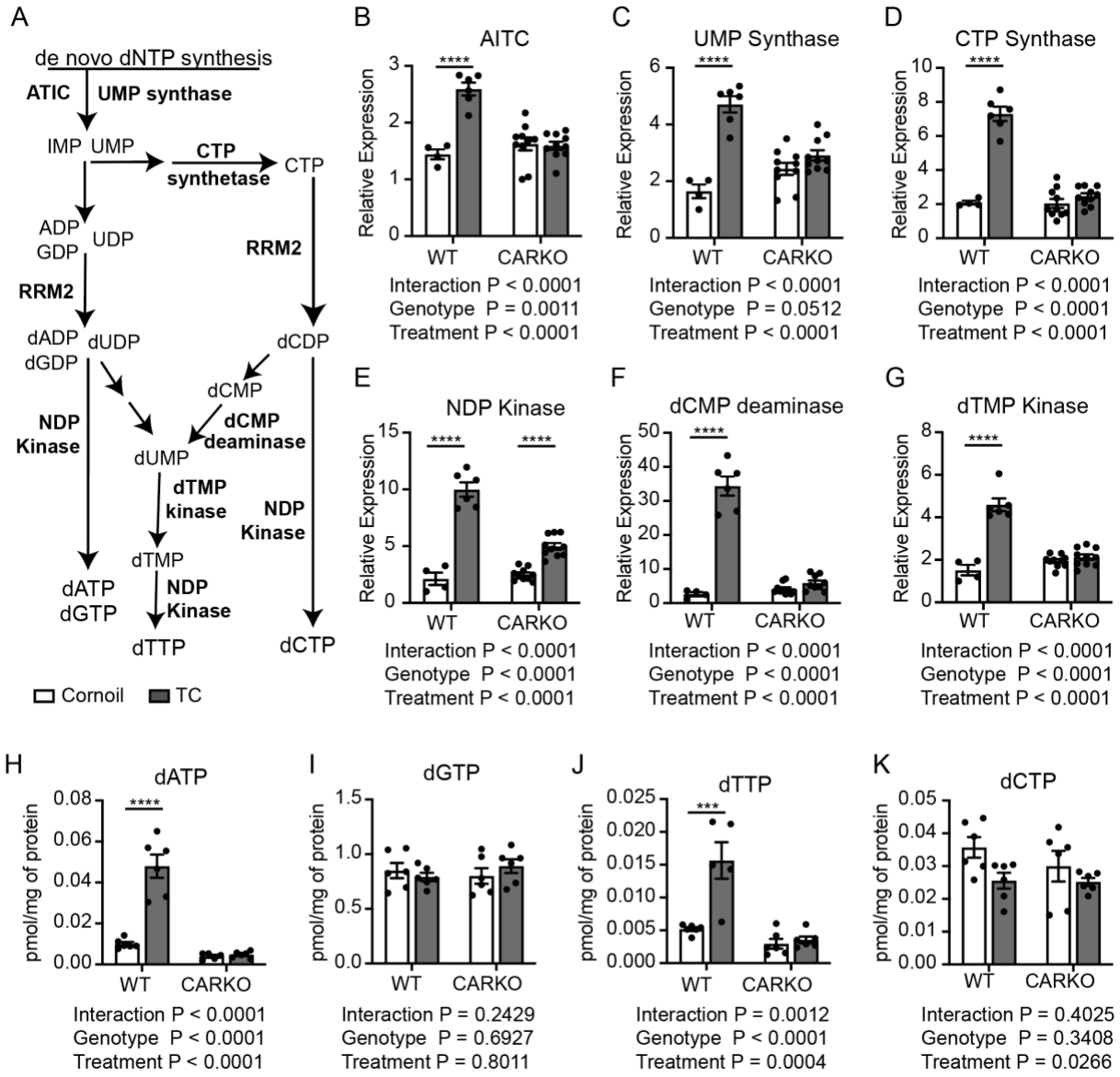

Figure 3. CAR activation increases key enzyme transcript levels in the *de novo* dNTP synthesis pathways. (A) Schematic representation of the crucial enzymes involved in the de novo dNTP synthesis pathway process. (B-G) Transcript levels of these enzymes – AITC (B), UMP Synthase (C), CTP Synthase (D), NDP Kinase (E), dCMP deaminase (F), dTMP Kinase (G) were measured using qPCR post-3-days of TC treatment. (n = 4-6, 3-month-old male mice, b-actin was used as the internal control for qPCR analysis). (H-K) Nucleotide (dATP (H), dGTP (I), dTTP (J), dCTP (K)) levels were analyzed from the liver tissue on CAR activation (n = 4-6 mice/group, 3-month male mice, normalized to the total protein of the liver sample).

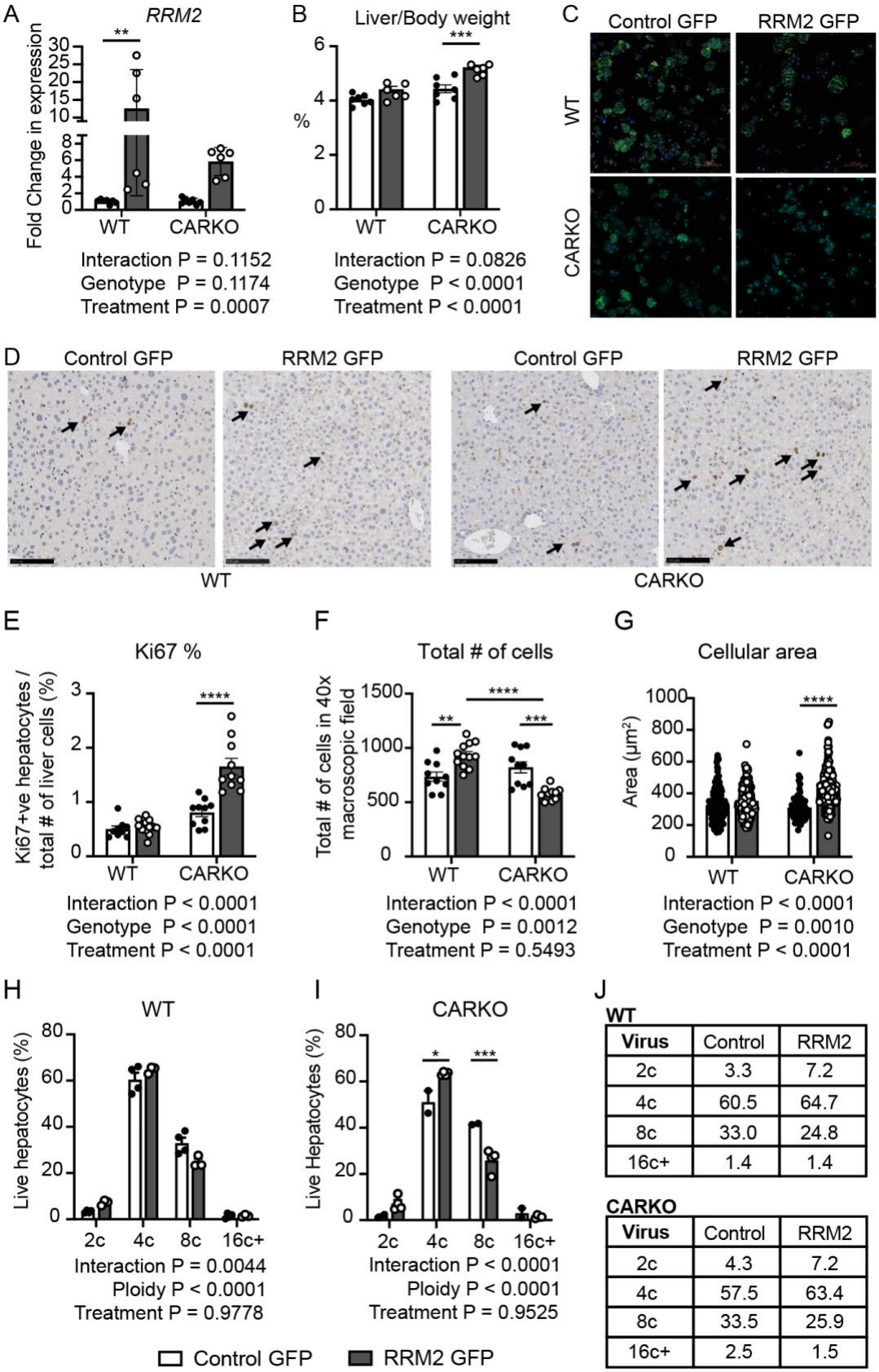

J

WT

Virus	Control	RRM2
2c	3.3	7.2
4c	60.5	64.7
8c	33.0	24.8
16c+	1.4	1.4

CARKO

Virus	Control	RRM2
2c	4.3	7.2
4c	57.5	63.4
8c	33.5	25.9
16c+	2.5	1.5

475

476 **Fig 4 – Overexpression of RRM2 in CARKO increases hepatocyte proliferation and alters**
477 **cellular ploidy.** (A) Transcript levels of *Rrm2* from WT and CARKO mice livers treated with
478 Control GFP or RRM2-GFP. (n = 6-8 mice/group, 4-month-old female mice, 36b4 was used as
479 the internal control for qPCR analysis). (B) The liver-to-body weight ratio for the virus-treated
480 mice. (C) Hepatocytes from mice treated with control-GFP and RRM2-GFP virus were isolated
481 with 2-step collagenase perfusion. These cells were incubated with DAPI (blue) and viewed
482 under a microscope for GFP or RRM2-GFP (green) expression. (D) Representative Ki-67 images
483 of WT and CARKO liver treated with control GFP or RRM2-GFP. Black arrows point to the Ki-
484 67 staining. (E) Quantification of Ki-67-positive hepatocytes in the liver section normalized to
485 the total number of cells under the focus region. (F) Total number of cells under the 40x
486 Microscopic field in the liver sections. (G) Liver sections were stained with β-catenin and DAPI,
487 and each cell's cellular area was measured with ImageJ software. (n = 6-8 mice/group, technical
488 replicate = 3 per group). (H-I) Cellular ploidy quantification for WT and CARKO with control
489 GFP or RRM2-GFP. Hepatocytes were isolated by 2-step collagenase perfusion and proceeded
490 for FACS sorting and ploidy analysis. (J) Average of cellular ploidy across 2-3 samples per
491 group.

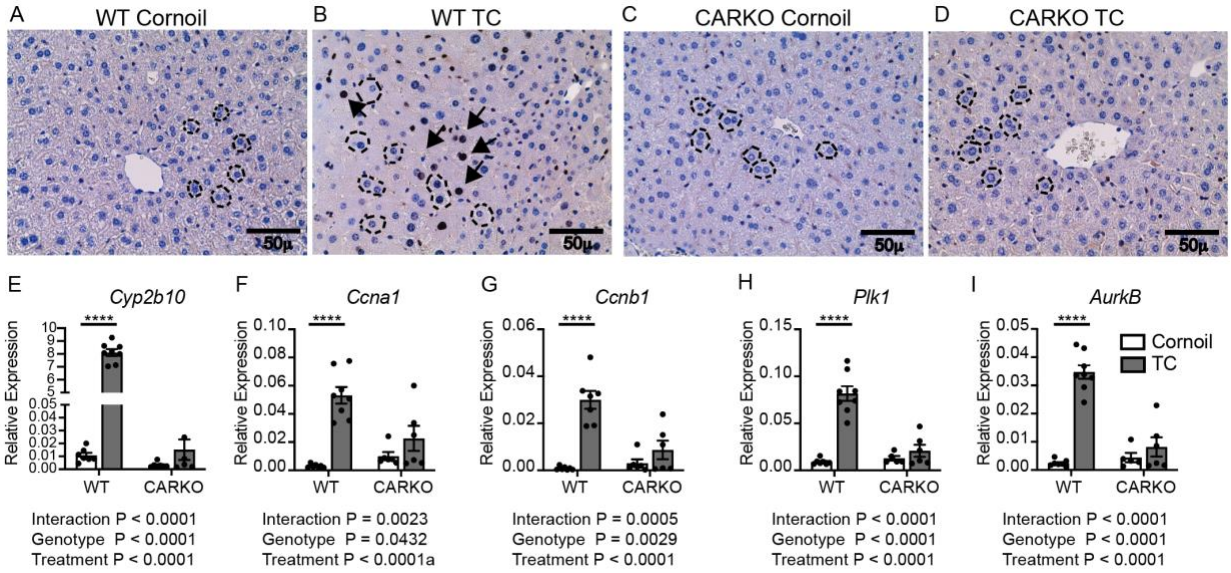

SI Figure 1 – CAR activation leads to an increase in Cyclins and mitotic entry genes. (A-D) Representative images of DNA synthesis marker, Ki-67 staining for WT (A and B) and CARKO (C and D) with and without TC treatment. The black arrow points to the Ki-67 staining and dotted line markers of the hepatocyte cell boundary. (E) CAR activation on TC treatment was determined by examining *Cyp2b10* transcript levels. (F-I) The Transcript levels of cyclins (*Ccna1*) and *Ccnb1*) and mitotic kinases (*Plk1* and *AurkB*) genes were analyzed using qPCR (n = 6-8 mice/group, adult male mice, 3-month-old, 36B4 was used as the internal control).

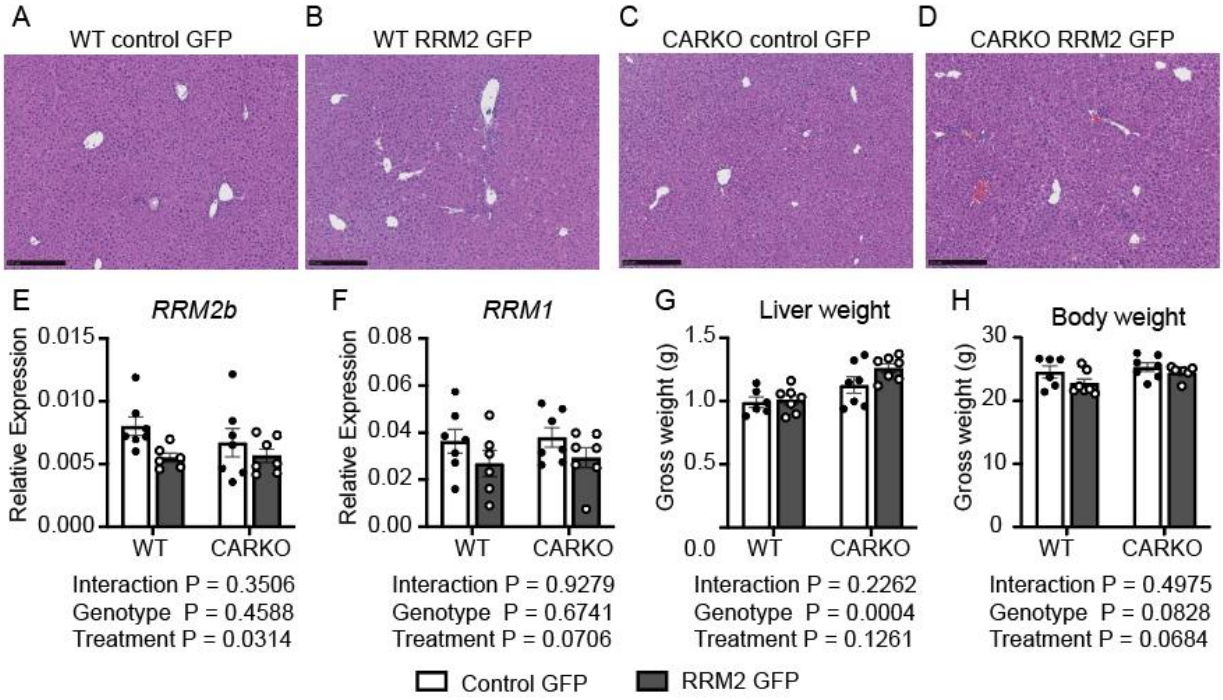

SI Figure 2 – AAV-based RRM2 overexpression did not induce inflammation or expression of other subunits of ribonucleotide reductase. (A-D) Representative H&E staining of WT and CARKO mice liver 2 weeks post-treatment with control GFP or RRM2-GFP. (E-F) Transcript levels of *Rrm2b* and *Rrm1* were analyzed from WT and CARKO mice livers under overexpression of RRM2 using qPCR. (n = 6-8 mice/group, 4-month-old female mice, 36b4 was used as the internal control for qPCR analysis). (G) Gross liver and body weight for the viral-treated mice.

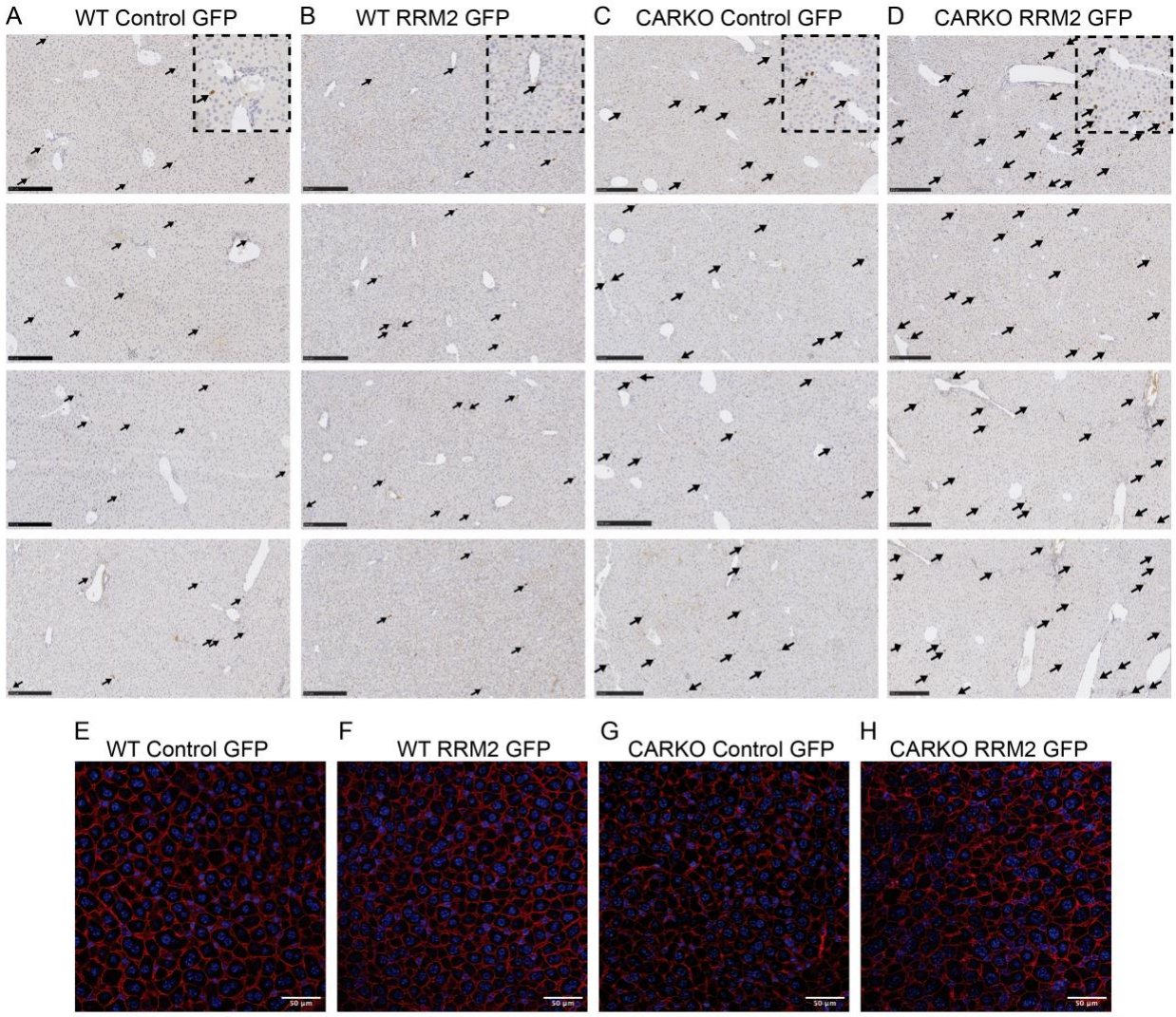

SI Figure 3 – Ki-67 and β-catenin staining for WT and CARKO liver with RRM2 overexpression. (A-D) Representative Ki-67 images of WT (A-B) AND CARKO (C-D) mice treated with Control-GFP (A and C) or RRM2-GFP (B and D) virus. Black arrows point to the Ki-67 stained using Immunohistochemistry. Enlarged images of Ki-67 staining are presented as insets in the upper panel of the figures on the right corner. (E-H) Representative images showing DAPI and β-catenin staining in control-GFP and RRM2-GFP for WT and CARKO mice livers. The hepatocyte area was measured using ImageJ software. (n = 6-10 mice/group)

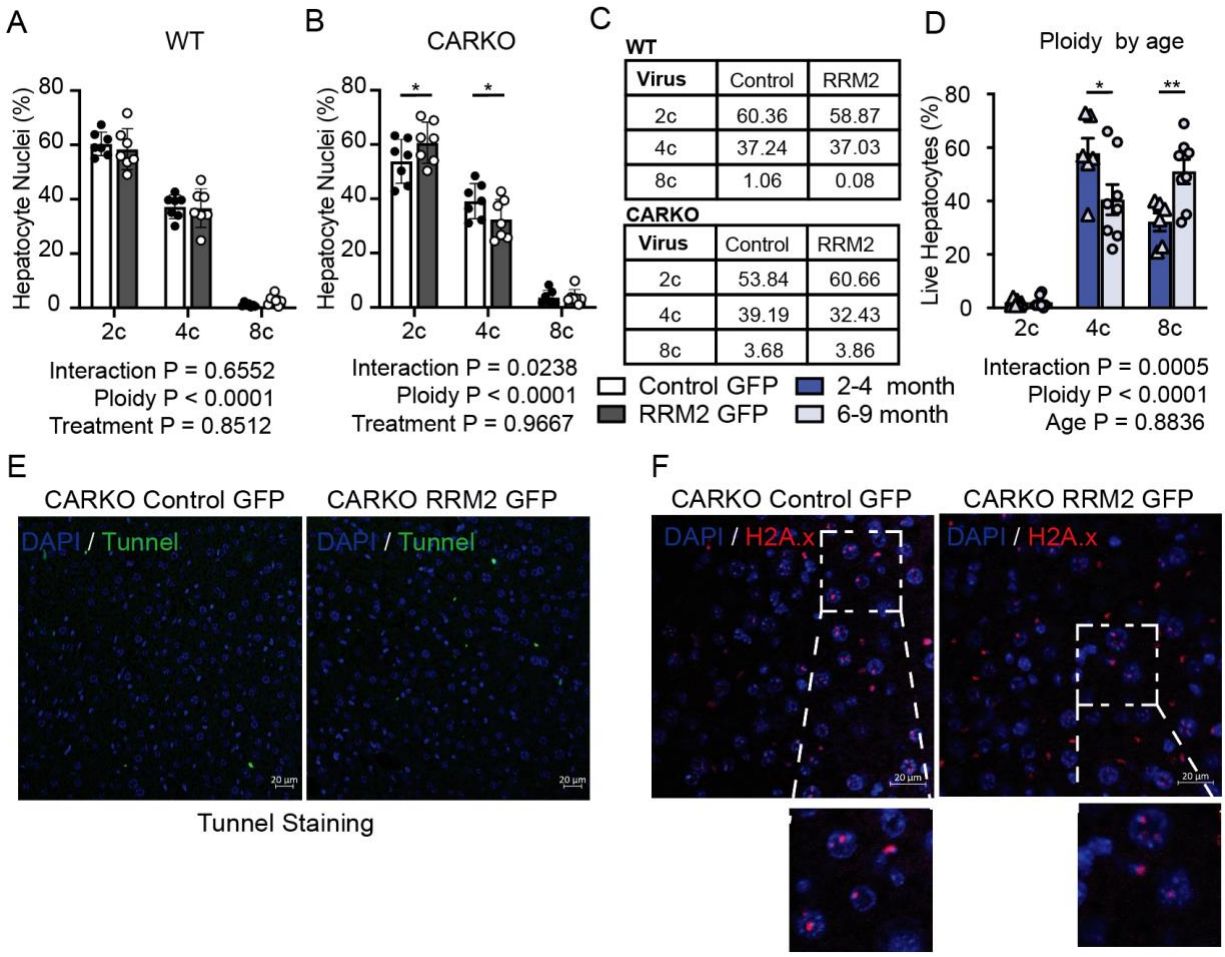

WT

Virus	Control	RRM2
2c	60.36	58.87
4c	37.24	37.03
8c	1.06	0.08

CARKO

Virus	Control	RRM2
2c	53.84	60.66
4c	39.19	32.43
8c	3.68	3.86

517

518 **SI Figure 4 – Overexpression of RRM2 rebuilds the lost ploidy in CARKO hepatocytes to**
519 **WT condition.** (A-B) Quantification for the liver nuclear ploidy analysis of WT and CARKO
520 mice under RRM2 overexpression, respectively (same sample set used for the gene expression
521 analysis to prevent batch error between the treatment groups, n = 7 mice/treatment group). (C)
522 Average nuclear ploidy analysis across 5-6 sample sets. (D) Age-dependent cellular ploidy
523 analysis from WT male mice. (n=6-8 mice/age). (E) Representative images of tunnel staining in
524 the CARKO control and RRM2 OE. (F) Representative images of H2A.x staining between the
525 control and RRM2 OE virus in CARKO mice.

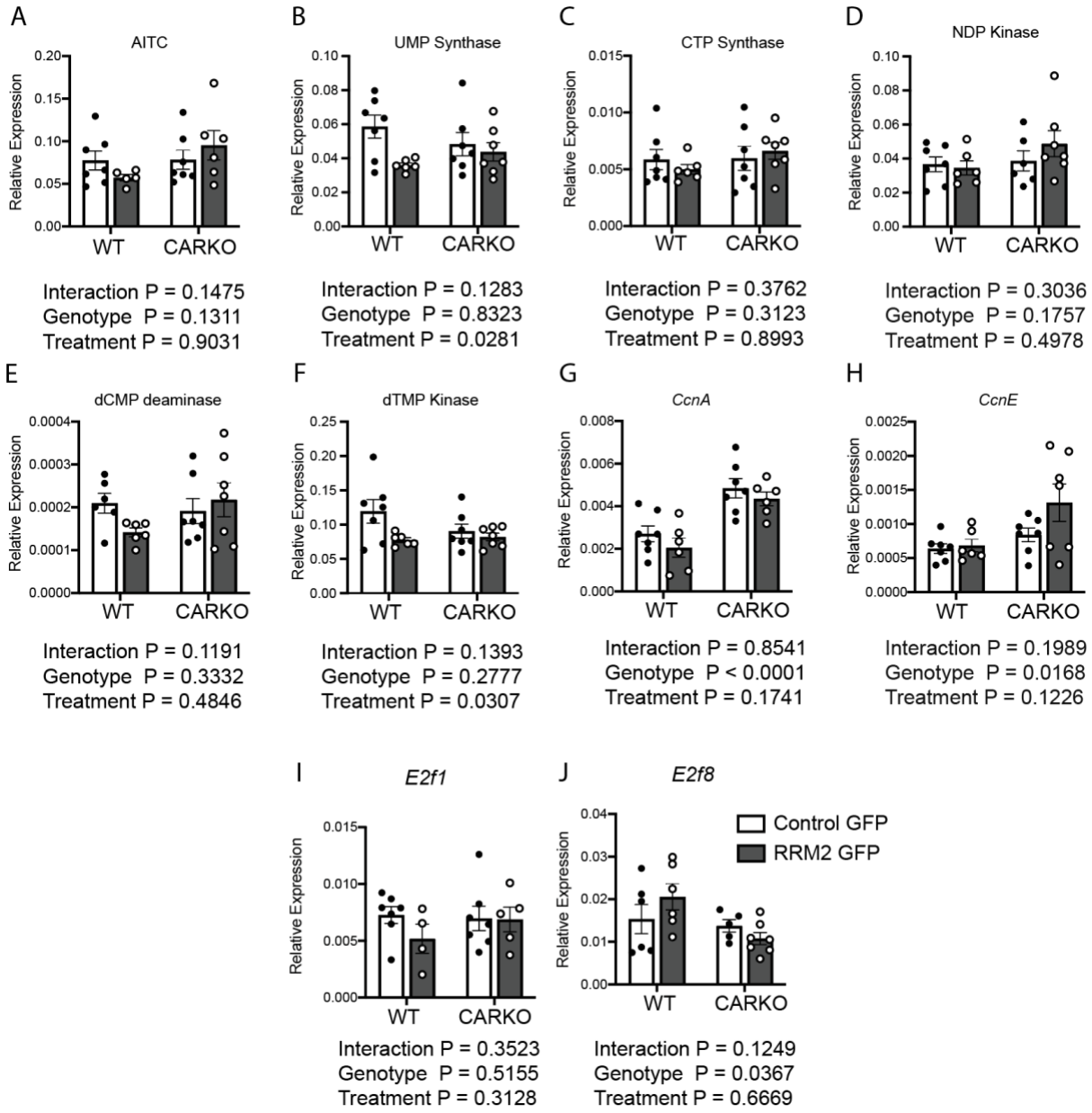

SI Figure 5 - No change in the enzyme and S and G2 cyclin transcript levels OR E2Fs after 2 weeks of RRM2 OE. qPCR analysis of A) AITC, B) UMP synthase, C) CTP synthase, D) NDP kinase, E) dCMP deaminase, F) dTMP Kinase, G) Cyclin A (*Ccna*), H) Cyclin E (*Ccne1*), (I) *E2f1* and (J) *E2f8* normalized to the internal control 36B4. There was no significant difference between the Control and RRM2 GFP treatment in WT or CARKO mice models

533 **Table 1 – List of primers used in this study**

Gene	Forward Primer (5'-3')	Reverse Primer (5'-3')
36B4	AGATGCAGCAGATCCGCAT	GTTCTTGCCCATCAGCACC
β-*actin*	TCTCCAGGGAGGAAGAGGAT	GCTACAGCTTCACCACCACA
Rrm1	ATGTGATCAAGCGAGATGGC	TTCATGGTGATCTGAGCAGG
Rrm2	GTTGTCTTTCCCATCGAGTACC	GAGCTTCCCAGTGCTGAATATC
Rrm2b	GAGCCACTCCTAAGAAAGAGTTC	GAGGGAGGTCCTTTGACAAGT
Cyp2b10	TGCTGTCGTTGAGCCAACC	CCACTAAACATTGGGCTTCCT
Ccna1	AGAAGACAAGCCAGTGAACG	GTCTGGTTGCCTCTTCATGT
Ccnb1	GCCAAGAGCCATGTGACTATC	CAGAGCTGGTACTTTGGTGTTC
Ccne1	GATCGTTACATGGCATCACA	AAACTGGTGCAACTTTGGAG
E2f1	ATCACCTCCCTCCACATCC	TGACAGTTGGTCCTCTTCCA
E2f8	GCAGTTGGAAGAGCAGTCAA	GCTGGATAAGGGACGGTGTA
Plk1	TTTGAGGTGGATGTGTGGTC	ACTGGGTTGATGTGCTTGG
Aurkb	GGATGTTGGGATGTTTCAGG	GGAGAAGAAGAGCCGTTTCA
AITC	TGTGGTCTGTAACCTGTACCC	CACGCCACCAATATCAATTTGTT
UMP	CAGTCAGGTCGCAGACATTTT	CCAGTGGTAACGCTGTATAAGGA
CTP	CTTTCTCCAGACTTAGTGGTGTG	ACCCGGTAGATGGATGAAACA
NDP	GAGGACTGCCGGAGGTTTTAC	GCAAGGATATAGGCTCGGATTG
dCMP	TCGAAGGAGCGGACGTGA	CTGACAAGAAGGCCACTGC
dTMP	TGCGTTTCCCCGAAAGATCAA	CCCAGCGGTTTGCAGAGAA

534